Valence band inversion and spin-orbit effects in the electronic structure of monolayer GaSe

Zeineb Ben Aziza, Viktor Zólyomi, Hugo Henck, Debora Pierucci, Mathieu G. Silly, José Avila, Samuel J. Magorrian, Julien Chaste, Chaoyu Chen, Mina Yoon, Kai Xiao, Fausto Sirotti, Maria C. Asensio, Emmanuel Lhuillier, Mahmoud Eddrief, Vladimir I. Fal'ko, and Abdelkarim Ouerghi

Valence Band Inversion and Spin-Orbit Effects in the Electronic Structure of Monolayer GaSe

Zeineb Ben Aziza[1], Viktor Zólyomi[2], Hugo Henck[1], Debora Pierucci[3], Mathieu G. Silly[4], José Avila[4], Samuel J. Magorrian[2], Julien Chaste[1], Chaoyu Chen[4], Mina Yoon[5,6], Kai Xiao[5], Fausto Sirotti[4], Maria C. Asensio[4], Emmanuel Lhuillier[7,8], Mahmoud Eddrief[7,8], Vladimir I. Fal'ko[2,*], and Abdelkarim Ouerghi[1,**]

[1] Centre de Nanosciences et de Nanotechnologies, CNRS, Univ. Paris-Sud, Université Paris-Saclay, C2N – Marcoussis, 91460 Marcoussis, France
[2] National Graphene Institute, University of Manchester, Manchester, M13 9PL, United Kingdom
[3] CELLS - ALBA Synchrotron Radiation Facility, Carrer de la Llum 2-26, 08290 Cerdanyola del Valles, Barcelona, Spain
[4] Synchrotron-SOLEIL & Université Paris-Saclay, Saint-Aubin, BP48, F91192 Gif sur Yvette Cedex, France
[5] Center for Nanophase Materials Sciences, Oak Ridge National Laboratory, Oak Ridge, Tennessee 37831, USA
[6] The University of Tennessee, Knoxville, Tennessee 37996, USA
[7] Sorbonne Universités, UPMC Univ. Paris 06, UMR 7588, INSP, F-75005 Paris, France
[8] CNRS, UMR 7588, Institut des NanoSciences de Paris (INSP), F-75005 Paris, France

*Corresponding author, E-mail: vladimir.falko@manchester.ac.uk

**Corresponding author, E-mail: abdelkarim.ouerghi@c2n.upsaclay.fr

Abstract:

Two-dimensional (2D) monochalcogenides (MX) have been identified as a unique and promising class of layered materials in recent years. The valence band of single layer MX_2, as predicted by theory, is inverted into a bow-shaped (often referred to as an inverted sombrero) and relatively flat dispersion, which is expected to give rise to strongly correlated effects. The inversion leads to an indirect band gap which is consistent with photoluminescence (PL) experiments, but PL provides no direct evidence of the band inversion in the valence band. Here we demonstrate for a hexagonal MX crystal, gallium selenide (GaSe), using a combination of angle-resolved photoemission spectroscopy (ARPES) and density functional theory (DFT), that the valence band of monolayer (ML) GaSe exhibits a robust inversion of the valence dispersion at the Γ point forming a bow-shaped dispersion with a depth of 120 ± 10 meV between the double valence band maximum (VBM) along the ΓK direction. We also demonstrate that the deeper lying bands detected in the ARPES spectrum are consistent with DFT calculations only if spin-orbit coupling is taken into account. The presented ARPES evidence that spin-orbit coupling leads to the splitting of two four-fold degenerate states into four Kramers doublets is of significant importance for PL measurements, as the change in energy of the second highest valence state at the Γ point has a measurable effect on the PL energies in high energy luminescence. We predict the optical absorption coefficients for the principal transitions in ML GaSe using a 4-band $\mathbf{k} \cdot \mathbf{p}$ model parametrized from first principles theory with spin-orbit effects taken into account.

Keywords: GaSe/graphene – ARPES – bow- shaped band structure – interlayer interaction – spin-orbit coupling

I. Introduction

Gallium selenide is a layered van der Waals (vdW) crystal in which the monolayer of the crystal consists of four atomic layers in the order of Se-Ga-Ga-Se. 2D crystals of GaSe have been used as active components in photodetectors[1,2], and GaSe also exhibits nonlinear optical behavior[3] which could potentially be utilized along with high mobility graphene within stacked vdW heterostructures[4]. Such vertical heterostructures have been heavily explored recently to create novel functionalities by combining different layered materials.[5,6]

What truly sets metal monochalcogenides like GaSe apart from the greater family of 2D materials is also the source of their aforementioned application potential in optoelectronics: their unique electronic structure. 2D materials offer several options for tunable electronic properties[7–9] through e.g. the evolution of the quasiparticle band gap as the number of layers changes, or by subjecting the films to doping and strain. A popular example of a family of 2D materials for such purpose are transition metal dichalcogenides (TMDs)[10–13], where the band edges are located at the corner of the Brillouin zone, and spin-orbit coupling leads to significant splitting at the VBM and CBM due to strong atomic spin-orbit coupling in transition metal atoms. Conversely, 2D monochalcogenides such as InSe[14–19], GaTe[15,20], GaSe[1–4,14,19,21,22], or their vertical heterostructures[23], have their band edges located at the Γ point and spin-orbit effects are much weaker. In particular, symmetry dictates that exactly at the Γ point the bands are spin-degenerate even with spin-orbit coupling taken into account. In addition, it has been shown theoretically that $M_{2N}X_{2N}$ films undergo a direct to indirect band gap transition when decreasing the number of layers N: from direct band gap in the bulk crystal to a weakly indirect gap for layers with N<7.[4] More specifically, by decreasing the number of layers, the conduction band minimum (CBM) remains at the Brillouin zone (BZ) center (Γ-point) while the valence band maximum slightly shifts away from the Γ towards the K point. This creates a bow-shaped valence band energy dispersion, sometimes referred to in the literature as an inverted sombrero function, resulting in a high density of states (DOS) and a Van Hove singularity near the valence band maximum (VBM). This unusual feature of the MX band structure can possibly lead to unconventional superconductivity or ferromagnetic phase transition according to recent theoretical studies.[24,25]

A less trivial but very much significant feature in MX materials is the presence of spin-orbit coupling. While compared to TMDs the effects of spin-orbit interaction on the band structure are not as pronounced due to the much smaller intrinsic spin-orbit coupling in group III metals compared to *e.g.* Mo or W, the symmetry breaking caused by this interaction has significant effects on both the electronic and optical properties of such 2D materials. As demonstrated in InSe[26], spin-orbit interaction promotes band mixing that activates otherwise forbidden optical transitions in monolayer MX crystals. Furthermore, spin-orbit effects lead to a splitting of the two, each fourfold degenerate bands just below the top valence band at the Γ-point into a total of four Kramers doublets (each of which retain their spin-degeneracy at the Γ-point as dictated by time reversal symmetry, and only split into spin-resolved bands at non-zero wave vectors). The magnitude of this splitting is on the order of several hundred meV and yields measurable differences in high energy photoluminescence transition energies when compared to theoretical predictions that neglect spin-orbit effects and are large enough to expect to be visible in ARPES.

In our previous work,[21] we obtained the first experimental ARPES observation of the bow-shaped valence band energy dispersion for 1-3 layer GaSe. Therein, we showed that sub-bands appear in the valence band structure when the number of layers in few-layer GaSe increases, while the band gap decreases. Here, we employ the fabrication technique established in Ref. 21 to prepare ML GaSe on two different substrates and explore in detail the valence band structure in ML GaSe near the VBM as well as deeper lying bands using ARPES experiments and first principles modeling. We demonstrate that spin-orbit coupling, although does not break spin degeneracy at the Γ-point, does lift band degeneracies in deeper lying valence bands, causing a splitting that is directly visible in the measured ARPES spectra even without spin-resolving the bands.

We investigate the role of the supporting substrate in doping GaSe as well as the charge transfer at the interface between the two materials. Reflection high-energy electron diffraction (RHEED) demonstrates that the structural properties of GaSe are preserved even when varying the doping of the graphene substrate from n-doped monolayer to approximately undoped bilayer. A noticeable upshift towards the Fermi level of the ML GaSe valence band is observed by ARPES when GaSe is grown on top of bilayer graphene compared to the case where n-doped monolayer graphene is used as a substrate. We determine the Schottky barrier height from the ARPES data on each substrate. Based on the ARPES evidence of spin-orbit related band splittings consistent with first principles, we provide a prediction for the optical absorption coefficients relevant to photoluminescence (PL), including high energy PL, in monolayer gallium selenide.

II. Methods

We used epitaxial graphene atop 6H-SiC(0001) surface to prepare a substrate in two configurations. First, we annealed the SiC crystal at 1550 °C in 800 mbar argon for 10 minutes, which produced a dead layer of carbon on the surface followed by a quasi-freestanding layer of graphene which presents an n-doping due to the presence of donor-like states associated with the buffer layer and its interface to the substrate,[27–30] and we found that the Fermi level (FL) was located approximately 0.3 eV above the Dirac crossing. This substrate shall be referred to as ML graphene. Second, we cut the substrate in half and exposed half of it to hydrogen using 100% H_2 at 820 °C for 10 minutes. This process transformed the buffer layer into a second graphene layer and reduced substantially the carrier concentration such that we obtained an approximately undoped bilayer (BL) graphene atop the SiC surface. This substrate shall be referred to as BL graphene. ARPES[31] was used to probe the band structure of both substrates for confirmation of the Dirac dispersion in the ML graphene and its modulation in the BL graphene (see Figure S1 in the Supplementary Material[32]).

Both the ML graphene and BL graphene substrates were annealed at 600 °C for 30 minutes in ultra-high vacuum to remove the residual surface contaminations induced by the air transfer. ML GaSe, formed of four atomic planes in the sequence of covalently bonded Se-Ga-Ga-Se, was grown following the method established in our previous work[21] directly on top of each substrate by vdW epitaxy (as shown in Figure 1(a)) using molecular beam epitaxy (MBE) under Se-rich conditions with the base pressure of 5×10^{-10} mbar. Elemental gallium (Ga) of 99.9% purity and selenium (Se) of 99.9% purity were used as the sources, and their fluxes were generated from a Knudsen cell. The substrate temperature during film deposition was fixed to ~350 °C. This

vdW epitaxy allows the combination of two layered materials with different properties even though they exhibit a large lattice mismatch.[33,34] In order to protect the GaSe from contamination and oxidation during transport in air to the ARPES end-station, a Se capping layer was deposited on the sample after the growth. For ARPES experiments, the Se capping layer was removed by annealing the sample at 250 °C in UHV for 40 min. The electronic properties of all samples were probed by ARPES experiments at ANTARES and TEMPO beamlines (SOLEIL French synchrotron facility). The used polarization configuration is illustrated in Figure S2 in the Supplementary Material[32].

We used RHEED to capture the diffraction patterns of both the ML graphene and the BL graphene substrates, as well as GaSe deposited on both substrates. In Figure 1(b), (c), (d) and (e), we show the typical RHEED patterns observed on the two graphene/SiC samples and GaSe/graphene/SiC, respectively. We note that Figure 1(b), corresponding to the RHEED of ML graphene/SiC, is similar to Figure 1(c) (BL graphene) except for some circular rays (highlighted by the red circle) related to the presence of the buffer layer in the n-doped ML graphene. One can clearly notice that in Figure 1(d) and (e) the patterns become blurrier compared to both graphene/SiC patterns due to GaSe deposition. Both patterns are identical implying the persistence of the structural properties of the grown GaSe on both graphene substrates. The appearance of the lines in the RHEED patterns of GaSe thin films suggests a well-ordered and flat surface. These images in Figure 1(d) and (e) show that the GaSe layers are epitaxially aligned with the graphene lattice showing uniform, smooth surfaces and interfaces with no reaction or intermixing. The streaky RHEED patterns in both [11-20] azimuth of GaSe films indicates that the two hexagonal unit cells are perfectly aligned such that [11-20]$_{GaSe}$//[11-20]$_{graphene}$ and [1-100]$_{GaSe}$//[1-100]$_{graphene}$ are in-plane. The additional streaks indicate also the presence of rotated 30° domains. Moreover, our RHEED images show that the two in-plane domain orientations of the GaSe layer are independent of the graphene layer doping. This hybrid GaSe/graphene interface is formed through van der Waals forces and does not involve covalent bonding. The RHEED patterns demonstrate that while interlayer interactions may alter the electronic structure of a 2D crystal deposited on a substrate[35,36], the atomic structure of GaSe is quite robust when switching between n-doped ML graphene and approximately undoped BL graphene substrates.
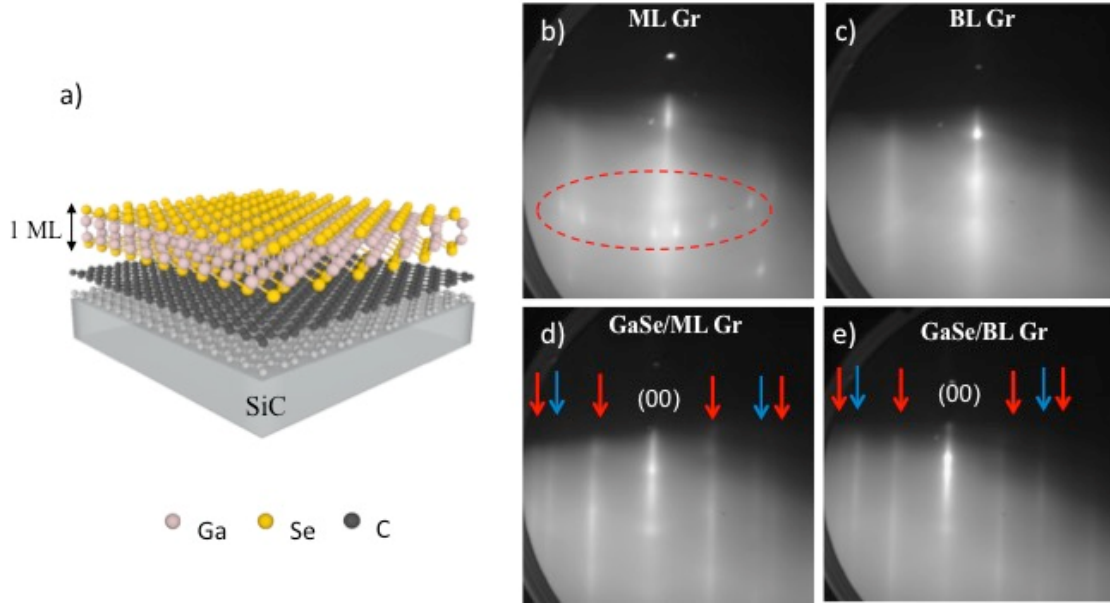
Figure 1: (a) Schematic of ML GaSe on epitaxial graphene/SiC, **(b) and (c)** RHEED patterns of ML and BL graphene/6H-Si(0001) (Gr) substrate, respectively, **(d) and (e)** streaky-line pattern during the GaSe growth process on ML and BL substrates, respectively. We note the simultaneous presence of rotated GaSe domains (two streak-lines pattern: red (0°) and blue (30°) arrows).

III. Results

We used ARPES to study the band structure of GaSe using an excitation energy hν = 60 eV. The ARPES maps for ML GaSe on ML graphene and on BL graphene are shown in Figure 2(a) and 2(b), respectively. These measurements agree quite well with data obtained previously on a different sample.[21,36] To enhance fine spectral features and get better clarity on the modification of the band structure, the second derivatives of the ARPES maps are presented in Figure 2(c) and 2(d), respectively. In red are shown our band structures calculated using the Perdew-Burke-Ernzerhof (PBE) implementation of the generalized-gradient approximation (GGA)[37] of density functional theory as realized in the VASP[38] code, with spin-orbit coupling taken into account (see Supplementary Material[32] for the computational details). As expected for ML GaSe, the upper valence band is represented by only one bow-shaped band. The measured depth at the center of the riser in the bow-shape, i.e. between the VBM at $k_{//}= 0.25$ Å^{-1} and the local valence band minimum at Γ is about 120 ±10 meV (obtained from energy distribution curves, see Figure S3 in the Supplementary Material[32]), which compares well with our theoretical value of 80 meV.
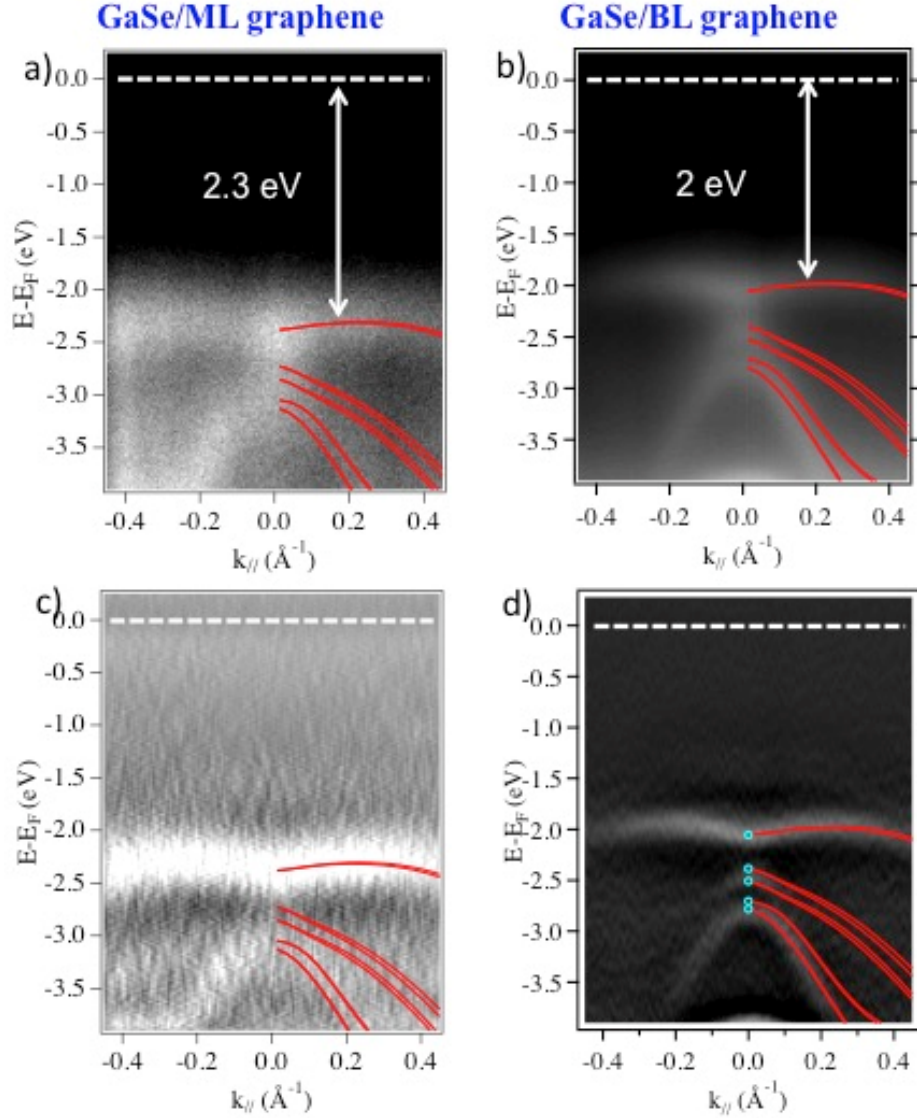
Figure 2: Electronic structure of ML GaSe/graphene heterostructures along the ΓK direction: (a) and (b) 2D ARPES spectra of ML GaSe grown on ML and BL graphene respectively, measured at hv = 60 eV and at T= 100 K, (c) and (d) second-derivative spectra of (a) and (b) for better visibility of the bands. White dotted lines indicate the Fermi Level position. The overlaid red lines are our DFT-calculated band structures using the PBE functional. The calculations include the effect of spin-orbit coupling and we also provide energies at the Gamma point from a k · p model (blue circles). The depth of the band inversion at the Γ-point is 120 ± 10 meV that compares well with the DFT value of 80 meV. The ARPES measurements have been performed at TEMPO (a) and ANTARES (b) beamlines (SOLEIL French synchrotron facility).

	E_{ARPES}	m^*_{ARPES}	E_{PBE}	m^*_{PBE}
VBM	0.12	-1.56	0.08	-1.90
Γ	0	0.65	0	0.86
Γ	-0.40	-0.30	-0.46	-0.29
Γ	- 0.79	-0.17	-0.73	-0.18

Table I: Comparison of band energies (eV) measured from the Γ –point energy in the top valence band (eV) and effective masses (m_e) in the ARPES measurements with DFT data using the PBE functional and taking spin-orbit coupling into account.

In our DFT calculations for the band structure of ML GaSe shown in Figure 2, spin-orbit coupling is taken into account. From this theory, we predict an electron-like effective mass at the Γ-point in the valence band with $m^* \approx$ 0.9 m_e and a hole-like effective mass at the VBM with $m^* \approx$ -1.9 m_e. This is in good agreement with the ARPES data (summarized in Table I), which yield an effective mass $m^* \approx$ 0.65 m_e at Γ and an effective mass $m^* \approx$ -1.56 m_e at the VBM. Effective masses in the deeper valence bands obtained by ARPES are in similarly good agreement with the calculations, with PBE predicting $m^* \approx$ -0.2 to -0.3 m_e in these bands (see Table S1 in the Supplementary Material[32] for more details). For comparison, in order to determine whether gradient effects, spin-orbit coupling, or exact exchange corrections are important for the quantitative description of the valence states, we also computed the band structure using the local density approximation (LDA) and the Heyd-Scuseria-Ernzerhof (HSE06) exact exchange functionals, where in the case of the former we included spin-orbit, and in the latter we neglected it. The LDA and HSE06 band structures are compared to the ARPES data in Figures 3(a) and (b), respectively. All of our calculations, along the ΓK direction, reproduce the measured highest valence band structure of ML GaSe. However, for lower lying bands, the best agreement is clearly found using the PBE functional (in Figure 2(d)), provided that spin-orbit coupling is taken into account. The HSE06 functional, in which 25% of the exchange interaction is treated exactly and tends to give a more precise description of electronic states than PBE, cannot reproduce the lower lying valence bands with the same accuracy, implying that the corrections from the exact exchange are negligible next to spin-orbit effects which we neglected in the HSE06 calculations. The LDA, from which generalized gradient corrections are missing (as opposed to PBE), predicts a much higher effective mass at the VBM, and both the LDA and HSE06 functionals give incorrect predictions for the Γ–point valence band energies relative to the top valence band (summarized in Table S1 in the Supplementary Information[32]). We conclude therefore, that in order to correctly describe the observed structure of lower lying valence bands in the measured ARPES spectra, it is necessary to take both gradient corrections and spin-orbit coupling into account.
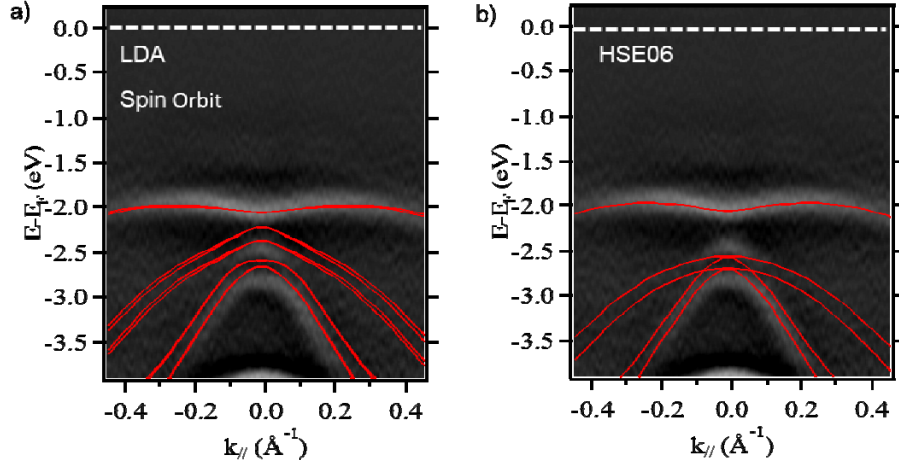
Figure 3: (a) and (b) density functional theory calculations for the valence band structure of ML GaSe compared with the measured second-derivative ARPES spectrum in Figure 2(d) using the LDA and HSE06 functionals, respectively. For LDA the spin-orbit coupling is included.

IV. Discussion

The ARPES observation of the valence band inversion agrees with previous DFT calculations[15], which have demonstrated the bow-shaped dispersion of the valence band for few layer III-VI materials such as GaSe, GaS, InS, and InSe. Subjecting GaSe to small amounts of p-doping creates a Fermi surface consisting of small, trigonally distorted circles around each of the VBM points in the Brillouin zone, i.e. one along each Γ-K line. Increasing the doping level eventually alters the topology of the Fermi surface upon reaching the saddle point along the Γ-M line, hence for large doping levels the Fermi surface consists of two concentric, hexagonally distorted circles with a very large diameter in **k**-space. This change of the Fermi surface topology is known as a Lifshitz transition[15]. The density of states at the saddle point is extremely large, giving rise to a Van Hove singularity. Since the VBM is not at the Γ–point and the conduction band minimum is at the Γ point, ML GaSe is an indirect band gap semiconductor. According to our measurements, the electronic structure of ML GaSe remains mostly unchanged when switching substrates except for a rigid shift of the overall electronic band structure.

The position of the VBM in the case of GaSe/ML graphene is located at a binding energy of -2.30±0.05 eV. In the case of ML GaSe/BL graphene an upshift of about 300 meV is observed. This suggests that the GaSe VBM is getting closer to the Fermi level and that GaSe tends to retrieve its p-type character,[36] which was completely lost in the ML GaSe/ML graphene where the substrate was heavily n-doped. Therefore, a possible explanation of this shift is a different charge transfer at the interface between the two-stacked materials depending on the graphene underlayer doping. In fact, changing the substrate doping corresponds to a variation of the band alignment between the two-layered materials. This band alignment in the case of n-type ML graphene promotes a charge transfer from graphene to the ML GaSe. The charge transfer is clearly reduced in the case of BL graphene, which is approximately undoped. This is the reason why the VBM, in this case, is approaching the

Fermi level (FL). Thus, changing the doping of the graphene underlayer is a viable method to reduce the induced n-type doping on GaSe grown on n-type ML graphene/SiC. It should be noted that in the case of the approximately undoped BL graphene substrate, the ML GaSe is still n-doped. Hence, the n-type doping from the substrate is not sufficient to explain the n-type character of ML GaSe. Then, this n-type doping of GaSe can partially originate from some defects such as Se vacancies (though we perform the growth process in a Se rich environment). However, the substrate has a strong impact on the modification of the as-grown GaSe doping.

The ARPES measurements of ML GaSe on ML and BL graphene show that the FL is located at around 2 and 2.3 eV above the maximum of the valence band. Given a 3.5 eV band gap for ML GaSe, obtained from scanning tunneling spectroscopy (STS) measurements[21], we can determine the Schottky barrier height (SBH) at the interface between graphene and the GaSe layer. The determination of SBH is of fundamental significance to the successful design of any device as it controls the electronic properties across the metal-semiconductor interface. Based on the ARPES data and the STS band gap, the SBH is about 1.2 and 1.5 eV for ML GaSe/ML graphene and ML GaSe/BL graphene, respectively. Based on these values, the band alignment diagrams of the GaSe/graphene heterostructures are derived and shown in Figure S4(a) and (b) in the Supplementary Material[32]. Our current findings are in accordance with the modulation of the GaSe electronic structure by the application of an external electric field (E_{ext}) reported by Si *et al*[39]. Indeed, they also observed that the valence band of ML GaSe/graphene gets closer to the FL by applying a positive E_{ext} perpendicular to the interface, *i.e.* p-doping. Moreover, the lack of dangling bonds on both materials ensures the absence of surface states and the formation of bonds at the interface[36]. This point is crucial to avoid a FL pinning allowing the formation of a quasi-ideal (semi)metal-semiconductor interface with a behavior approaching the Schottky limit.[40] Consequently, the SBH at the interface between the graphene FL and the GaSe VBM decreases resulting in a tunable potential step. These findings demonstrate that the modulation of the interface dipole in the heterostructure can be easily controlled by the substrate doping without altering their structural properties of the 2D materials as confirmed by the RHEED.

The spin-orbit induced band splitting in lower lying valence bands in MX chalcogenides is of significance as they are involved in higher energy PL transitions, where during absorption an electron is promoted to the bottom of the conduction band from the lower lying valence state, and recombination is enabled by a suppression of electron-phonon and Auger processes between the valence states[19]. From the DFT band structure of ML GaSe it is possible to extract parameters for a 4-band $\mathbf{k} \cdot \mathbf{p}$ model of GaSe near the Γ-point, based on a similar model of InSe[26]. Such a model enables us to make a prediction for the absorption coefficients of optical transitions.

In this approach we approximate the conduction band (*c*) as a quadratic function, the valence band (*v*) as an isotropic fourth order polynomial, and deeper lying occupied bands (v_1, v_2) as quadratic functions. The Hamiltonian takes the form of

$$
\hat{H} = \begin{bmatrix}
H_c \mathbb{1}_s & E_z d_z & \frac{e\beta_1}{cm_e} \mathbb{1}_s \otimes \mathbf{A} & \lambda_{c,v_2} \hat{\mathbf{s}} \\
E_z d_z & H_v \mathbb{1}_s & \lambda_{v,v_1} \hat{\mathbf{s}} & \frac{e\beta_2}{cm_e} \mathbb{1}_s \otimes \mathbf{A} \\
\frac{e\beta_1}{cm_e} \mathbb{1}_s \otimes \mathbf{A^T} & \lambda_{v,v_1} \hat{\mathbf{s}}^{\mathbf{T}} & \mathbb{1}_s \otimes \mathbf{H}_{v_1} + \lambda_{v_1} s_z \otimes \sigma_y & 0 \\
\lambda_{c,v_2} \hat{\mathbf{s}}^{\mathbf{T}} & \frac{e\beta_2}{cm_e} \mathbb{1}_s \otimes \mathbf{A^T} & 0 & \mathbb{1}_s \otimes \mathbf{H}_{v_2} + \lambda_{v_2} s_z \otimes \sigma_y
\end{bmatrix};
$$

$$H_c \approx E_c + \frac{\hbar^2 k^2}{2m_c}; \; H_v \approx E_v + E_2 k^2 + E_4 k^4; \; \mathbf{H}_{v_{1(2)}} \approx \left[E_{v_{1(2)}} + \frac{\hbar^2 k^2}{2m_{1(2)}}\right]\mathbb{1}_\sigma + \frac{\hbar^2\left(k_x^2 - k_y^2\right)}{2m'_{1(2)}}\sigma_z + \frac{2\hbar^2 k_x k_y}{2m'_{1(2)}}\sigma_x.$$

Here the basis is of spin up/down states in the bands $\{c, v, v_1, v_2\}$. The values of the $\mathbf{k}\cdot\mathbf{p}$ parameters, summarized in Table II, are obtained from fitting to scissor corrected DFT dispersions without spin-orbit coupling near the Γ point. $\mathbf{H}_{v_{1(2)}}$ are 2-component Hamiltonians written as matrices in a space of p_x, p_y orbitals, with $\mathbb{1}_\sigma$ being the identity matrix, and $\sigma_{x,y,z}$ the Pauli matrices. The factors $\frac{e\beta_{1(2)}}{cm_e}$ are couplings of the spin-conserving interband optical transitions between c and v_1 and between v and v_2, respectively, to in-plane polarized light described by vector potential $\mathbf{A}$. The matrix element $E_z d_z$ accounts for electric dipole coupling of the principal interband transition to out-of-plane polarized light. In the spin space $\mathbb{1}_s$ is the identity matrix, while $s_{x,y,z}$ are spin operators, with $\hat{\mathbf{s}} \equiv (s_x, s_y)$ and $\hat{\mathbf{s}}^T \equiv \begin{pmatrix} s_x \\ s_y \end{pmatrix}$. The parameters $\lambda_{v_{1(2)}}, \lambda_{v,v_1}, \lambda_{c,v_2}$ are spin-orbit coupling constants in a band basis, obtained from fitting to scissor corrected DFT energies at Γ with spin-orbit coupling taken into account. The effect of λ_{c,v_2} on the analysis is neglected due to the large energy difference between the bands involved.

From this, we can calculate the optical absorption coefficients at Γ using the formulas[26]

$$g_A(E_z)[\theta \approx 45°] = 8\pi\frac{e^2}{\hbar c}|d_z/e|^2\frac{\hbar\omega m_c}{\hbar^2}; \; g_B(\sigma^\pm) = 8\pi\frac{e^2}{\hbar c}|\beta_1|^2\frac{m_c}{\hbar\omega m_e^2}; \; g_A(\sigma^\pm) = 8\pi\frac{e^2}{\hbar c}|\beta_{sf}|^2\frac{m_c}{\hbar\omega m_e^2}$$

where the first two absorption coefficients are for the transitions allowed even in the absence of spin-orbit coupling, and are for the coupling of the principal interband transition (A line) to out-of-plane polarized light incident at $\theta \approx 45°$, and for the coupling of the higher energy PL transition (B line) to in-plane polarized light incident perpendicular to the crystal, respectively, as shown in Figure 4. $\hbar\omega$ is the energy difference between the bands involved in the transition, and m_c is the conduction band effective mass. $g_A(\sigma^\pm)$ gives the absorption coefficient for the coupling of the principal interband transition to in-plane polarized light, which is forbidden in the absence of spin-orbit coupling, with $|\beta_{sf}|^2 = |\delta C_v(v_1)\beta_1|^2$ determined by the weight of v_1 band p_x, p_y orbitals admixed into the valence band wavefunction by spin-orbit coupling, $|\delta C_v(v_1)|^2$. This yields the following prediction for the absorption coefficients of monolayer gallium selenide:

$$g_A(E_z)[\theta \approx 45°] = 3.5\%; \; g_B(\sigma^\pm) = 9.3\%; \; g_A(\sigma^\pm) = 0.7\%.$$

The most significant absorption is therefore expected for the higher energy PL transition, while the lowest energy transition with in-plane polarized light enabled by spin-orbit coupling gives a much smaller, but non-zero contribution to absorption, implying that with a suitable setup both transitions should be possible to observe in experiments.
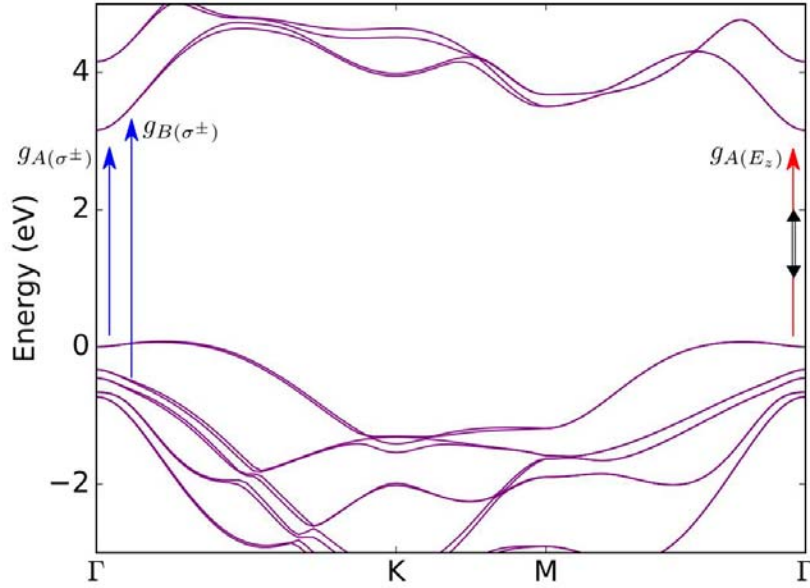
Figure 4: Optical transitions in ML GaSe illustrated on the scissor corrected DFT band structure of ML GaSe. The band structure was obtained using the PBE functional with spin-orbit coupling taken into account, and scissor correction was based on a comparison of the measured and calculated band gap in the bulk crystal. The A transition corresponds to the lowest energy transition which may be activated by out-of-plane polarization or by in-plane, where the latter is only made possible by spin-orbit interaction. The B transition corresponds to high-energy luminescence for in-plane polarization.

The Γ–point band energies summarized in Table II can be compared to transport experiments. The measured STS gap[21] of 3.5 eV is quite close to the calculated vertical energy gap of 3.24 eV. The difference between the two can be ascribed to the scissor correction, which is performed by rigidly shifting the occupied bands by the difference between the measured and calculated band gap of the bulk phase. While this approach has been proven to work very well for PL gaps in InSe films[14,19], it does neglect the dependence of the scissor correction on the number of layers, which leads to errors on the order of 0.1 eV for the monolayer energy gap, which is an acceptable error next to a band gap of 3.5 eV. Note that in our $\mathbf{k} \cdot \mathbf{p}$ model we use the scissor correction since PBE both underestimates the band gap and does not take the thermal shift into account. The purpose of the $\mathbf{k} \cdot \mathbf{p}$ model is to provide predictions for photoluminescence measurements, which are typically performed at room temperature. Therefore, we implement a scissor correction by comparing the PBE bulk band gap to the experimental room temperature gap and adding the difference between the two to the band energies of all unoccupied states in the band structure. This method of scissor correction has been demonstrated to predict quite well the PL gaps of InSe films.[2]

Hamiltonian $\mathbf{k}\cdot\mathbf{p}$ parameters				$\mathbf{k}\cdot\mathbf{p}$ Γ-point band energies with SOC	
E_c	3.24 eV	m_c	$0.16\,m_e$	$E_c^{\pm\frac{1}{2}}$	3.24 eV
E_v	−0.05 eV	m_1'	$-0.36\,m_e$	$E_v^{\pm\frac{1}{2}}$	0 eV
E_2	4.18 eVÅ^2	m_2'	$-0.33\,m_e$	$E_{v_1}^{\pm\frac{3}{2}}$	−0.33 eV
E_4	−38.9 eVÅ^4	β_1	1.25 ħ/Å	$E_{v_1}^{\pm\frac{1}{2}}$	−0.65 eV
E_{v_1}	−0.47 eV	d_z	1.62 eÅ	$E_{v_2}^{\pm\frac{3}{2}}$	−0.46 eV
E_{v_2}	−0.59 eV	λ_{v_1}	0.27 eV	$E_{v_2}^{\pm\frac{1}{2}}$	−0.73 eV
m_1	$-0.26\,m_e$	λ_{v_2}	0.27 eV		
m_2	$-0.23\,m_e$	λ_{v,v_1}	0.23 eV		

Table II: Parameters of the $\mathbf{k}\cdot\mathbf{p}$ Hamiltonian, with the zero-level set to $E_v^{\pm\frac{1}{2}}$.

V. Conclusions

In summary, we have presented a combined experimental and theoretical investigation of the structure and the electronic band structure of ML GaSe using RHEED, ARPES, and first principles modeling. We performed a detailed analysis of the top valence band, which exhibits an inversion near the zone center with a depth of 120 ± 10 meV. We have shown that the ARPES spectra are consistent with first principles density functional theory only if spin-orbit coupling is taken into account, revealing the importance of spin-orbit interaction for lower lying occupied bands. We found that changing the substrate modulates the band alignment between GaSe and the substrate resulting in a rigid shift of the bands of GaSe without any significant changes in its structure. We have provided predictions for the optical absorption coefficients of ML GaSe using a $\mathbf{k}\cdot\mathbf{p}$ model parameterized from density functional theory.

References

1. Lu, R., Liu, J., Luo, H., Chikan, V. & Wu, J. Z. Graphene / GaSe-Nanosheet Hybrid : Towards High Gain and Fast Photoresponse. *Sci. Rep.* **6,** 1–7 (2016).

2. Hu, P., Wen, Z., Wang, L., Tan, P. & Xiao, K. Synthesis of few-layer GaSe nanosheets for high performance photodetectors. *ACS Nano* **6,** 5988–5994 (2012).

3. Allakhverdiev, K. R., Yetis, M. Ö., Özbek, S., Baykara, T. K. & Salaev, E. Y. Effective nonlinear GaSe crystal. Optical properties and applications. *Laser Phys.* **19,** 1092–1104 (2009).

4. Li, X. *et al.* Controlled Vapor Phase Growth of Single Crystalline, Two-Dimensional GaSe Crystals with High Photoresponse. *Sci. Rep.* **4,** 5497 (2014).

5. Geim, A. K. & Grigorieva, I. V. Van der Waals heterostructures. *Nature* **499,** 419–425 (2013).

6. Britnell, L. *et al.* Strong Light-Matter Interactions in heterostructures of atomically Thin Films. *Science (80-.).* **340,** 1331–1314 (2013).

7. Novoselov, K. S., Mishchenko, A., Carvalho, A., Neto, A. H. C. & Road, O. 2D materials and van der Waals heterostructures. *Science (80-.).* **353,** aac9439 (2016).

8. Li, X. Q. and Y. W. and W. L. and J. L. and J. *et al.* Modelling of stacked 2D materials and devices. *2D Mater.* **2,** 32003 (2015).

9. Bhimanapati, G. R. *et al.* Recent Advances in Two-Dimensional Materials beyond Graphene. *ACS Nano* **9,** 11509–11539 (2015).

10. Pierucci, D. *et al.* Large area molybdenum disulphide-epitaxial graphene vertical Van der Waals heterostructures. *Sci. Rep.* **6,** 26656 (2016).

11. Mouri, S., Miyauchi, Y. & Matsuda, K. Tunable photoluminescence of monolayer MoS2 via chemical doping. *Nano Lett.* **13,** 5944–5948 (2013).

12. Conley, H. J. *et al.* Bandgap Engineering of Strained Monolayer and Bilayer MoS 2. *Nano Lett.* **13,** 3626–3630 (2013).

13. Ben Aziza, Z. *et al.* Bandgap inhomogeneity of MoS 2 monolayer on epitaxial graphene bilayer in van der Waals p-n junction. *Carbon N. Y.* **110,** 396–403 (2016).

14. Magorrian, S. J., Zólyomi, V. & Fal'Ko, V. I. Electronic and optical properties of two-dimensional InSe from a DFT-parametrized tight-binding model. *Phys. Rev. B* **94,** 1–20 (2016).

15. Zolyomi, V., Drummond, N. D. & Fal'Ko, V. I. Band structure and optical transitions in atomic layers of hexagonal gallium chalcogenides. *Phys. Rev. B - Condens. Matter Mater. Phys.* **87,** 1–6 (2013).

16. Mudd, G. W. G. et al *et al.* High Broad-Band Photoresponsivity of Mechanically Formed InSe–Graphene van der Waals Heterostructures. *Adv. Mater.* **27,** 3760–3766 (2015).

17. Mudd, G. W. *et al.* Quantum confined acceptors and donors in InSe nanosheets. *Appl. Phys. Lett.* **105,** (2014).

18. Velichko, A. et al V *et al.* Highly-mismatched InAs/InSe heterojunction diodes. *Appl. Phys. Lett.* **109,** 182115 (2016).

19. Bandurin, D. A. *et al.* High electron mobility, quantum Hall effect and anomalous optical response in atomically thin InSe. *Nat. Nanotechnol.* **12,** 223–227 (2017).

20. Liu, F. *et al.* High-Sensitivity Photodetectors Based on Multilayer GaTe Flakes. *ACS Nano* **8,** 752–760 (2014).

21. Ben Aziza, Z. *et al.* Tunable quasiparticle band gap in few-layer GaSe / graphene van der Waals

heterostructures. *Phys. Rev. B* **96,** 45404 (2017).

22. Tamalampudi, S. R. *et al.* High Performance and Bendable Few-Layered InSe Photodetectors with Broad Spectral Response. *Nano Lett.* **14,** 2800–2806 (2014).

23. Wang, F. Y. and L. Z. and A. P. and P. H. and X. W. and W. L. and D. Z. and Q. L. and Q. F. and C. S. and K. C. and L. E. and K. & Faguang Y et al. Fast, multicolor photodetection with graphene-contacted p -GaSe/ n -InSe van der Waals heterostructures. *Nanotechnology* **28,** 27LT01 (2017).

24. Wu, X. *et al.* Magnetisms in p-type monolayer gallium chalcogenides (GaSe, GaS). *arXiv:1409.4733v2.* 1–6 (2014).

25. Cao, T., Li, Z. & Louie, S. G. Tunable Magnetism and Half-Metallicity in Hole-doped Monolayer GaSe. *Phys. Rev. Lett.* **114,** 236602 (2015).

26. Magorrian, S. J.; Zólyomi, V. Fal'ko, V. I. . Spin-orbit coupling, optical transitions, and spin pumping in mono- and few-layer InSe. *Submitt. to Phys. Rev. B*

27. Ouerghi, a. *et al.* Epitaxial graphene on 3C-SiC(111) pseudosubstrate: Structural and electronic properties. *Phys. Rev. B* **82,** 125445 (2010).

28. Mallet, P. *et al.* Electron states of mono- and bilayer graphene on SiC probed by scanning-tunneling microscopy. *Phys. Rev. B - Condens. Matter Mater. Phys.* **76,** 1–4 (2007).

29. Kopylov, S., Tzalenchuk, A., Kubatkin, S. & Fal'Ko, V. I. Charge transfer between epitaxial graphene and silicon carbide. . *Appl. Phys. Lett.* **97,** 11–14 (2010).

30. Ristein, J., Mammadov, S. & Seyller, T. Origin of doping in quasi-free-standing graphene on silicon carbide. *Phys. Rev. Lett.* **108,** 1–5 (2012).

31. Henck, H. *et al.* Electrolytic phototransistor based on graphene-MoS2 van der Waals p-n heterojunction with tunable photoresponse p-n heterojunction with tunable photoresponse. *Appl. Phys. Lett.* **109,** 113103 (2016).

32. See Supplemental Material at http://.

33. Koma, A. Van der Waals epitaxy for highly lattice-mismatched systems. *J. Cryst. Growth* **201,** 236–241 (1999).

34. Lang, O., Tomm, Y., Schlaf, R., Pettenkofer, C. & Jaegermann, W. Single crystalline GaSe/WSe2 heterointerfaces grown by van der Waals epitaxy. II. Junction characterization. *J. Appl. Phys.* **75,** 7814–7820 (1994).

35. Pierucci, D. *et al.* Band alignment and minigaps in monolayer MoS2-graphene van der Waals heterostructures. *Nano Lett.* **16,** 4054–4061 (2016).

36. Ben Aziza, Z. *et al.* van der Waals Epitaxy of GaSe/Graphene Heterostructure: Electronic and Interfacial Properties. *ACS Nano* **10,** 9679−9686 (2016).

37. Perdew, J. P., Burke, K. & Ernzerhof, M. Generalized Gradient Approximation Made Simple. *Phys. Rev. Lett.* **77,** 3865–3868 (1996).

38. Kresse, G.; Furthmüller, J. Efficient iterative schemes for ab initio total-energy calculations using a plane-wave basis set. *Phys. Rev. B* **54,** 11169 (1996).

39. Si, C., Lin, Z., Zhou, J. & Sun, Z. Controllable Schottky barrier in GaSe/graphene heterostructure: the role of interface dipole. *2D Mater.* **4,** 15027 (2016).

40. Quang, T. Le *et al.* Scanning tunneling spectroscopy of van der waals graphene/semiconductor interfaces: absence of Fermi level pinning. *2D Mater.* **4,** 35019 (2017).